

Evaluation of direct-quadrature position and saturation of a SynRM machine with Segmented Rotor

M. Shahril Anwar¹, Mohd Azri Hizami Rasid^{1,*}

¹Faculty of Manufacturing and Mechatronics Engineering Technology, Universiti Malaysia Pahang, 26600 Pahang, Malaysia.

ABSTRACT – The synchronous reluctance machine has gained popularity in traction and other smaller application thanks to its design that need very little or even no permanent magnet. Without internal permanent magnet assistance, an adequate level of torque density could be achieved by having an optimized rotor design to attain the optimum ratio of direct inductance over quadrature inductance. In order to properly control the machine, the direct and quadrature position need to be identified. In this study, a segmented rotor topology without permanent magnet was chosen. We evaluate the direct and quadrature position of the rotor topology, its saturation level and provide the flux linkage and the inductances of the machine.

ARTICLE HISTORY

Received: 27th July 2022

Revised: 2nd Sept 2022

Accepted: 4th Oct 2022

KEYWORDS

SynRM

Direct-quadrature position

Inductances

Flux linkage

Saturation

INTRODUCTION

Reducing the amount of permanent magnet integrated into an electrical machine is indisputably important. It serves the purposes of reducing the cost and increasing the reliability in high temperature operating condition. Synchronous Reluctance machine (SynRM) fulfils this requirement with several options of rotor topologies [1-3].

The SynRM torque is produced by the reluctance principle, where the flux crosses the air gap presents the least reluctance path, while pulling its load. The saliency ratio, which is the difference of inductance in direct position and quadrature position defines the intensity of the torque produced. This can be explained by Equation (1) [4].

$$\Gamma_{max} = \frac{3}{2}p(L_d - L_q)I_s^2 \sin 2\beta \quad (1)$$

where L_d and L_q represent the direct and quadrature inductance respectively. p is the number of pair of poles, I_s is the RMS current, and β the load angle. The load angle is defined as the angle between the current and the direct axis in the machine phasor diagram [5]. It can be seen that as the higher the saliency ratio, the higher the torque will be.

There are four major types of SynRM rotor topology that can be found in literature [3]. Figure 1 shows them. The simple salient pole and segmented rotor are simple and easy to fabricate. The segmented rotor has a higher saliency ratio in comparison to simple salient pole. The flux-barrier rotor is the most employed in industry due to its highest saliency ratio. The pattern stamped onto the rotor laminations conduct the flux in a way to creates a high saliency ratio.

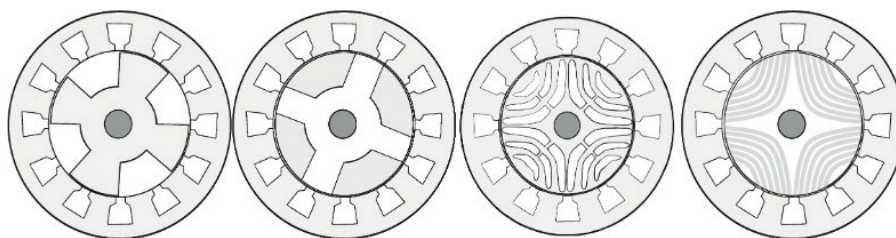


Figure 1. Different rotor topology for SynRM machine. From left to right: simple salient pole, segmented rotor, flux-barrier rotor, axially laminated rotor.

In all cases, to design a SynRM machine, it is important to evaluate the direct and quadrature inductance, (L_d , L_q) to predict the torque that can be produced. To properly control the motor to get the maximum torque, the position of L_d , L_q also need to be precisely identified to be able to position the control load angle. Therefore, we propose a preliminary

study to evaluate the position of direct and quadrature axis of a SynRM with segmented rotor, and we will evaluate the saturation level, the inductance and flux linkage of the machine that is produced by each phase using FE analysis tool.

SYNRM DEFINITION AND FE MODEL

In this study, we have chosen to design a SynRM with segmented rotor with a constraint in the outer dimension. The machine is intended to be used where it could be integrated into a small volume. It was designed to serve the function of an automotive clutch actuator [6]. The constraints are the external stator diameter which is D_{stat_extat} 43.40 mm and the machine length which is l_u at 70mm. Due to constraints in terms of fabrication, we chose the segmented rotor and 4 poles design. The other dimensions are as shown in the Figure 2.

Dimension parameters		Values
D_{shaft}	Rotor shaft diameter	6.00 mm
$D_{int\ stat}$	Stator interior diameter	25.24 mm
$D_{ext\ stat}$	Stator exterior diameter	43.40 mm
D_{wire}	Wire diameter	0.60 mm
$D_{int\ stat}$	Stator interior diameter	26.04 mm
e	Air gap	0.40 mm
e_{shim}	Slot chin thickness	1.00 mm
e_{casing}	Casing thickness	0.80 mm
$h_{stat\ yoke}$	Rotor yoke height	3.40 mm
l_{tooth}	Tooth width	3.40 mm
$l_{non\ mag}$	Rotor nonmagnetic part width	2.21 mm
l_{fan}	Teeth fanning width	5.62 mm
$l_{slot\ opening}$	Slot opening width	1.19 mm
l_u	Active length	70.00 mm
N_{wire}	Number of wire	Number of wire
N_{slot}	Number of slots	12
p	Number of pole pair	2

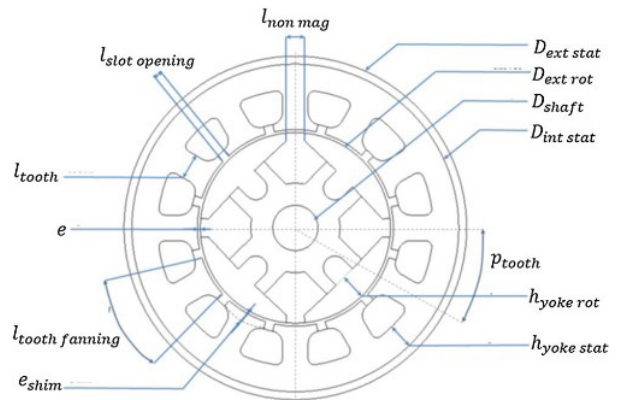


Figure 2. The design and dimension of the SynRM with segmented rotor.

The study is conducted using FE analysis tool, FEMM. The complete geometry of the machine was drawn with the proper material assigned to its proper region (Figure 3). The material list for each part of the machine. The ferromagnetic rotor segment and the stator core are made of M14 magnetic steel lamination, while the segment hold, the shaft and the casing are made of aluminium for lightness and heat conductivity.

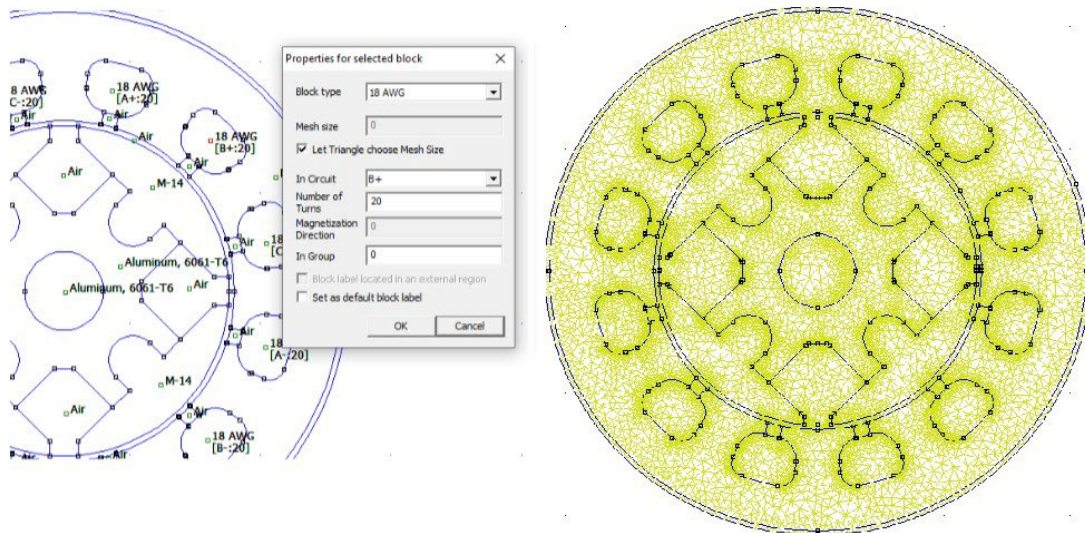


Figure 3. The material assigned to the area, circuit definition and meshing of the SynRM model.

The meshing was done using triangular surface mesh with automatic variable mesh size (the corners contain more triangles, thus resolution to observe the eventual magnetic saturations). The boundary conditions on the outer circumference of the casing were set as zero flux crossing. The solver used was in 2D planar and magneto-static setting.

The electrical circuit was defined as 3 phase distributed winding. The material as shown in Figure 3 is copper, using a 18AWG conductor size, with 20 as number of turns. The meshing and simulation parameters to evaluate the L_d , L_q position is done as shown in Table 2. To identify the direct and quadrature position, a static 3-phase current was fed to the stator while rotating the rotor for a quarter rotation. This is sufficient thanks to the symmetry of the 4-pole machine. The resolution of the rotation is at each 5-degree angle. To observe the saturation effect, the current tested ranges up to 20A. For reference, 20 A is the common current limit for a battery in steady state continuous utilization.

To assess the saturation level, the maximum flux density value is collected in direct position L_d for currents ranging from 1A to 20A. This will allow us to observe the decrease of slope of flux density in relation to the current increase.

Finally, the inductance per phase and flux linkage per phase is taken from the post- processor of the FE tools.

RESULTS AND DISCUSSIONS

Direct and quadrature position

Graph in Figure 5 below shows the variation of maximum flux density on the machine as the rotor are being rotated for a quarter turn, for different current level. The maximum flux density is achieved when the rotor is at 0 degree and repeats for each quarter rotations. At 90 degrees, the maximum flux density can once again be observed. This indicates the direct position of the rotor. On the other hand, the minimum flux density which indicates the quadrature position of the rotor can be observed when the rotor is at 45-degree position. As the current increases, we remark that the flux density plot gets closer to each other, that may indicate the beginning of saturation.

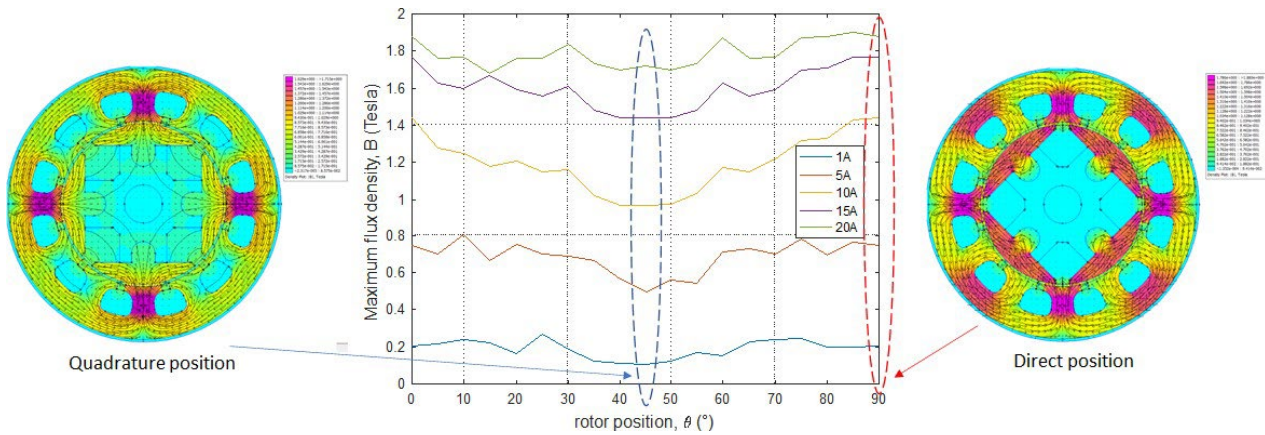


Figure 4. Identification of direct and quadrature position of the rotor at different current level.

Saturation level

To observe the saturation effect clearer, we plot the magnetization curve of the machine. Figure 6 shows the plot of maximum flux density as the current increases, but only at two positions of the rotor which are the L_d , L_q position. In both cases, the increase of flux density is linear up to between 10A and 15A. After that, the flux density increase or slope start to reduce, entering a plateau of saturation. Flux density at L_d tops at 1.88T while at L_q tops at 1.72T. L_q is linear in comparison to L_d . This is due to the flux path in quadrature position passing mostly through air gaps which is not affected by saturation. In direct position however, the flux passes mostly through the core material that is made of M14 soft magnetic steel, that inherently possess a saturation characteristic. Therefore, we could expect nonlinearity as well in the increases of torque as the current is increased.

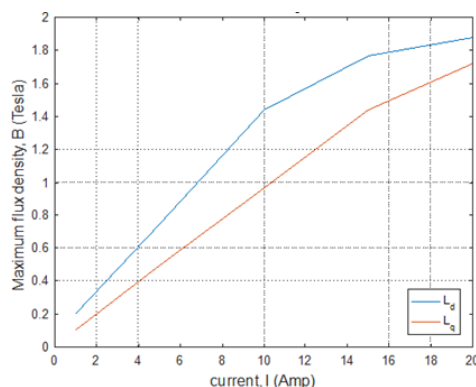


Figure 5. The magnetization curve, plotted on maximum flux density for direct and quadrature position.

Inductances direct and quadrature

For inductances, Figure 7 shows the inductance generated inside the machine. The three graphs on the left represents the inductances created by each phase of the winding as a with regards to the current and angle of rotation. Across the angle of rotation, the balanced triphase currents produced balanced sinusoidal inductance distribution with a lag of 2π between each phase. With regards to the current, across all phases, the inductances vary differently. The graph on the right of Figure 7 is the variation of inductance, taken specifically at direct and quadrature position. In a balanced triphase, it can be seen that inductance for phase a and c are equal. For all phases, the quadrature inductances maintain its values while for direct inductance, its value decreases imaging the fact of saturation discussed previously. This is because the inductance is defined as amount of flux produced per current. Therefore, as the flux increase starts to slow down in with regards to the increase of current, the inductance in consequence will be reduced. If we consider the linear region, the maximum inductance which occurs in phase a are $L_{d,a} = 1.28 \times 10^{-3}$ and $L_{q,a} = 0.32 \times 10^{-3}$. Due to saturation, at 20 A the inductance in phase a drop to $L_d = 0.91 \times 10^{-3}$, while $L_{q,a}$ maintains constant.

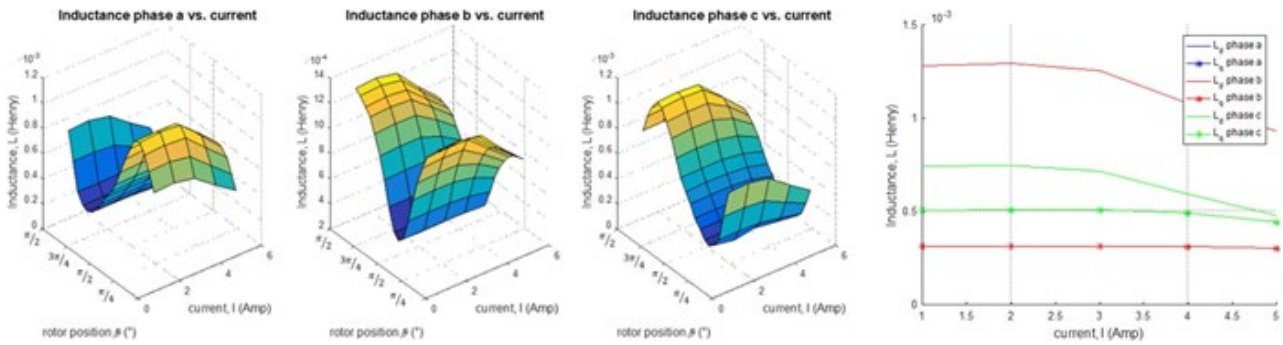


Figure 6. Left: Inductance on each phase, a, b, and c as function of rotor position and current. Right: Inductance on each phase for direct and quadrature position.

Flux linkages

As for flux linkage, Figure 8 below shows the flux linkage produced by each phase. The same observation as inductance can be made regarding the form of the inductance surface with regards to rotor position and current. With the figure on the right of Figure 8, we can see that for each phase, the direct flux linkage experience saturation as the current increases while the quadrature flux linkage maintains a constant slope as the current increases.

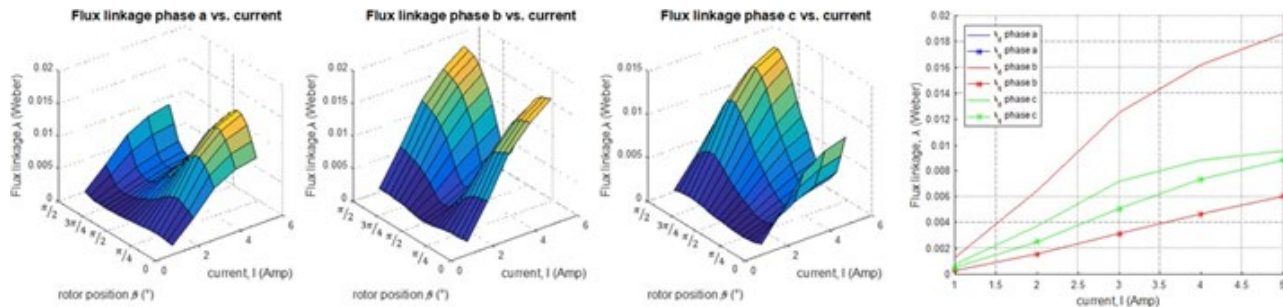


Figure 7. Left: Flux linkage generated by each phase, a, b and c as function of rotor position and current. Right: Flux linkage each phase for direct and quadrature position.

CONCLUSION AND PERSPECTIVES

In this study, a SynRM machine with segmented rotor FE model was developed to evaluate its direct-quadrature rotor position and evaluate its saturation level. The choice of segmented rotor size of the machine was limited by an external dimension constraint. The direct and quadrature position where the direct inductance L_d and the quadrature inductance L_q can be computed are located at 0 rad and π rad with repetition at each π rad. The resulting inductances are found to be at $L_{d,a} = 1.28 \times 10^{-3}$ and $L_{q,a} = 0.32 \times 10^{-3}$ generated by phase a. Due to saturation, at 20 A the inductance in phase a drops to $L_d = 0.91 \times 10^{-3}$, while $L_{q,a}$ maintains constant. The saturation effect on direct inductance is therefore non-negligible and will have an impact on the torque produced. In perspective, near future works will consists of calculating

the direct and quadrature inductances form the phase inductances, and then compute the torque produced. To maintain the torque increase by eliminating saturation effect, we could either improve the geometry of the machine (by enlarging the saturated area observed) or find another magnetic material that has a higher saturation level.

ACKNOWLEDGEMENT

The authors would like to thank UMP for funding this work under an internal grant RDU220302.

REFERENCES

- [1] A. A. Arkadan, A. A. Hanbali and N. Al-Aawar, "Design Optimization of ALA Rotor SynRM Drives Using T-AI-EM Environment," in *IEEE Transactions on Magnetics*, vol. 43, no. 4, pp. 1645-1648, April 2007, doi: 10.1109/TMAG.2007.892493.
- [2] Y. Hu, B. Chen, Y. Xiao, J. Shi, X. Li and L. Li, "Rotor Design and Optimization of a Three-Phase Line-Start Synchronous Reluctance Motor," in *IEEE Transactions on Industry Applications*, vol. 57, no. 2, pp. 1365-1374, March-April 2021, doi: 10.1109/TIA.2020.3043224.
- [3] Rasid, M.A.H., Lanfranchi, V., Ospina, A. et al. Torque Ripple Analysis of Synchronous Reluctance Motor with Different Rotor Topologies for Application with Dimensional Constraint. *J. Electr. Eng. Technol.* 15, 2167–2177 (2020). <https://doi.org/10.1007/s42835-020-00493-8>
- [4] T. A. Lipo and P. C. Krause, "Stability Analysis of a Reluctance-Synchronous Machine," in *IEEE Transactions on Power Apparatus and Systems*, vol. PAS-86, no. 7, pp. 825-834, July 1967, doi: 10.1109/TPAS.1967.291749.
- [5] Boldea, I., & Tutelea, L. (2018). *Reluctance Electric Machines: Design and Control* (1st ed.). CRC Press. <https://doi.org/10.1201/9780429458316>
- [6] M. A. H. Rasid, A. Ospina, K. El Kadri Benkara and V. Lanfranchi, "A thermal study on small synchronous reluctance machine in automotive cycle," 2016 IEEE 25th International Symposium on Industrial Electronics (ISIE), 2016, pp. 134-140, doi: 10.1109/ISIE.2016.7744879.